



ELSEVIER

Available online at [www.sciencedirect.com](http://www.sciencedirect.com)

ScienceDirect

Energy Procedia 102 (2016) 70 – 79

Energy

Procedia

E-MRS Spring Meeting 2016 Symposium T - Advanced materials and characterization techniques  
for solar cells III, 2-6 May 2016, Lille, France

## Annealing of Thin-film Cadmium Telluride Photovoltaics Using Holographically Controlled Laser Processing

Nicholas Goffin<sup>\*a</sup>, Fabiana Lisco<sup>b</sup>, Gianfranco Claudio<sup>b</sup>, John Tyrer<sup>c</sup>, Elliot Woolley<sup>a</sup>

<sup>a</sup>Centre for Sustainable Manufacturing and Recycling Technologies (SMART), Wolfson School of Mechanical and Manufacturing Engineering,  
Loughborough University, LE11 3TU, UK

<sup>b</sup>Centre for Renewable Energy Systems Technology (CREST), School of Electronic, Electrical and Systems Engineering, Loughborough  
University, Leicestershire, LE11 3TU, UK

<sup>c</sup>Optical Engineering Research Group, Wolfson School of Mechanical and Manufacturing Engineering, Loughborough University, LE11 3TU,  
UK

---

### Abstract

CdTe-based thin film solar cells currently represent one of the fastest growing PV technologies, with a superior combination of efficiency, energy payback time and lifecycle environmental impact. However, the current post-deposition annealing treatment is still an energy intensive step of the manufacturing process. A novel method is presented for annealing of CdTe using a high-power diode laser (35 W, 808 nm) for thermal post-processing, combined with holographic optical elements (HOE's) for laser beam heat flow control. The advantage of a laser for annealing lies in its ability to selectively heat only the surface of the CdTe solar cell; improving energy efficiency, process speed and energy resilience. Heat transfer simulations were used to predict the effects of different laser irradiance profiles on the annealing process thermal cycle influence the experimental design and predict optimal laser irradiance profiles. Variations in power and process speed on as-deposited and MgCl<sub>2</sub>-treated close-space sublimated (CSS) CdTe samples have been performed. The results were characterised using scanning electron microscopy (SEM), transmission electron microscopy (TEM) and X-ray photoelectron spectroscopy (XPS). Optical properties were analysed with a spectrophotometer and ellipsometric spectroscopy (SE). The laser annealing treatment was found to be effective in promoting Chlorine diffusion and improving the optical and morphological properties of CdTe thin film devices.

© 2016 The Authors. Published by Elsevier Ltd. This is an open access article under the CC BY-NC-ND license (<http://creativecommons.org/licenses/by-nc-nd/4.0/>).

Peer-review under responsibility of The European Materials Research Society (E-MRS).

---

<sup>\*</sup> Corresponding author. Tel.: +44-01509-225403  
E-mail address: [n.goffin@lboro.ac.uk](mailto:n.goffin@lboro.ac.uk)

*Keywords:* thin-film, laser annealing, holographic optics, recrystallisation, cadmium telluride

## 1 Introduction

The band gap of Cadmium Telluride (CdTe), at approximately 1.45 eV is optimal for terrestrial solar radiation [1]. The absorption co-efficient at these wavelengths is high enough that a CdTe layer with a 1  $\mu\text{m}$  thickness can absorb over 90% of incident photons [2]. Layer thicknesses of maximum 3  $\mu\text{m}$  are therefore easily sufficient for terrestrial panels. A critical component in CdTe efficiency is grain size, along with the presence of voids and stacking faults [3]. Factors that affect this include the structure and deposition technique for the preceding Cadmium Sulphide (CdS) layer [4] and the deposition temperature [5].

CdTe photovoltaics currently require an activation treatment, by thermal annealing in the presence of Chlorine; generally applied in the form of Cadmium Chloride ( $\text{CdCl}_2$ ), or with more recent experiments in the form of Magnesium Chloride ( $\text{MgCl}_2$ ) [6]. This requires temperatures of around 400 - 450°C. The use of  $\text{CdCl}_2$  promotes recrystallisation and efficiency improvements.  $\text{MgCl}_2$  has been investigated as a means of avoiding the severe health and safety issues associated with  $\text{CdCl}_2$ .

Numerous experiments have been completed for the CdTe annealing process, with various results [7–10]. This oven treatment requires a high temperature to be maintained for a set time, making it slow and vulnerable to fluctuations in energy supplies. This also requires the heating of the entire panel in order to process a thin surface layer of photosensitive material. It is possible that the use of a laser-based alternative heat source could produce improvements over conventional annealing.

### 1.1 Lasers in CdTe annealing

Lasers can provide certain advantages, such as localised heat treatment, selective annealing, short process duration times and precision control of the heating time [11].

Previous work has been completed in this area. Kim *et al.* [12] used an 808 nm diode laser to anneal CdTe thin films. 808 nm is the optimal wavelength, since the photon energy of the laser light needs to be high enough for the beam to be absorbed by the CdTe (wavelength below 850 nm), but not so high that the beam is absorbed without penetrating into the substrate. Use of this method by Kim *et al.* gave recrystallisation and grain growth with heating times in the region of 15 seconds.

In the laser process thus far described, limitations have been identified. Lasers are known to generate a high thermal gradient due to the tight control of the heat flux; this property is what makes them so useful in metallic laser welding [13]. For processing of photovoltaic panels with glass substrates this property is not beneficial, since the brittleness of glass causes it to shatter when exposed to these gradients. In the previously mentioned literature, this is avoided by rapid-scanning of the beam over a large area in order to more gently heat the substrate using multiple passes; achieved via use of a galvanometer head. This avoids the issues with thermal gradient, but is limited in scalability due to the fact that the area that can be covered is limited by the size of the galvanometer.

### 1.2 Holographic Optical Elements in laser materials processing

In this study, investigations of the use of customised laser beams are presented as a way of controlling heat flow. Standard laser beams suffer from disadvantages regarding their thermal profiles, which contribute to the previously mentioned thermal gradient issues due to the fact that the irradiance profile of the laser beam directly affects the thermal cycle of the processed material [13]. Standard laser beams are described as  $\text{TEM}_{00}$  beams, with a circular spot and Gaussian thermal profile, as shown in Figure 1. These Gaussian beam shapes create a concentration of temperature in the centre of the beam, causing uneven heating in the material. This creates the large thermal

gradients which cause cracking, as well as unevenly processing the surface of the panel.

To mitigate this, customised beams can be created by use of a novel type of optic called a Holographic Optical Element (HOE). This uses a computer-generated kinoform to reshape a laser beam into any desired thermal profile. A schematic of how this works is shown in Figure 1.

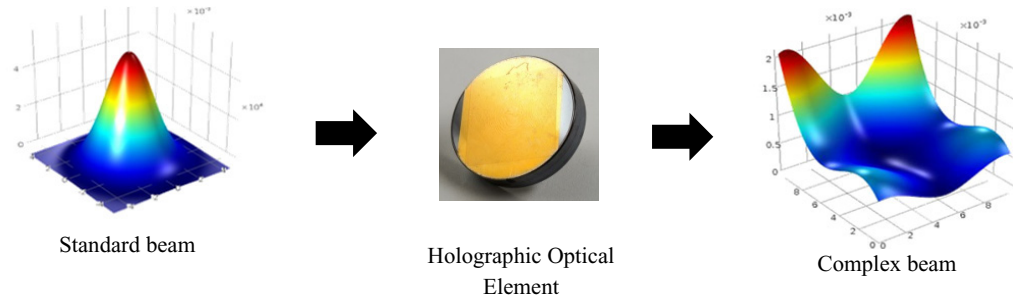


Figure 1: Schematic of the principles of holographic control of laser beam profile

The typical method of laser experimentation, where the process has to be adapted to account for a non-optimised beam, therefore no longer applies. HOE's have been investigated in a number of laser processing applications, such as laser welding [14] and wire-based laser deposition [15].

In this work, holographic laser annealing is investigated in both simulation and experimental conditions. Simulations are used to demonstrate the alterations of heat flow caused when the beam thermal distribution is optimised. Initial experimental results created using a Gaussian beam are then presented, which demonstrate the capabilities of laser annealing for CdTe processing.

## 2 Simulation setup

The COMSOL Multiphysics simulation software was used for heat transfer simulations. Three different beam types of diameter 5 mm were simulated. These are shown in Figure 2.

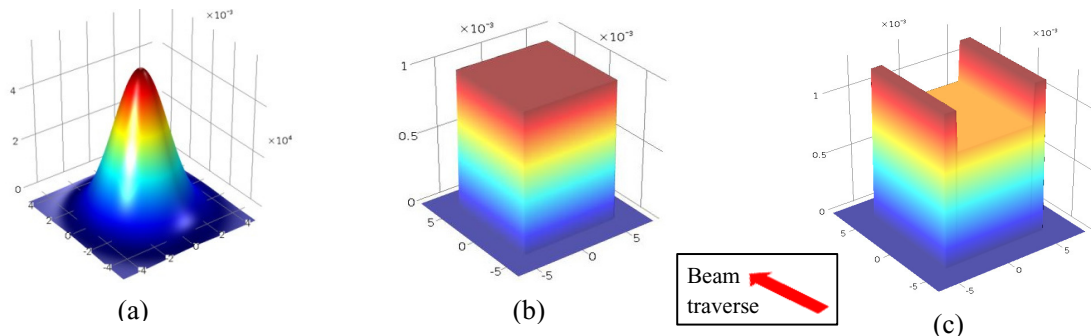


Figure 2: Beam profile plots of (a) 5 mm diameter Gaussian beam (b) 5 x 5 mm pedestal beam (c) 5 x 5 mm rugby posts beam

The Gaussian beam in Figure 2a is the standard  $TEM_{00}$  beam used in most laser applications. In Figure 2b, a “pedestal” beam is applied that corrects the two major flaws of the Gaussian beam; it has a square footprint and a uniform thermal profile. These flaws were described in detail by Goffin *et al.* [15]. Figure 2c shows a further refinement of the pedestal beam, called a “rugby posts” beam. This places additional heat at the edges of the laser

beam to compensate for heat losses there.

In order to minimise computing time, a 20 x 20 mm sample was modelled (Figure 3).

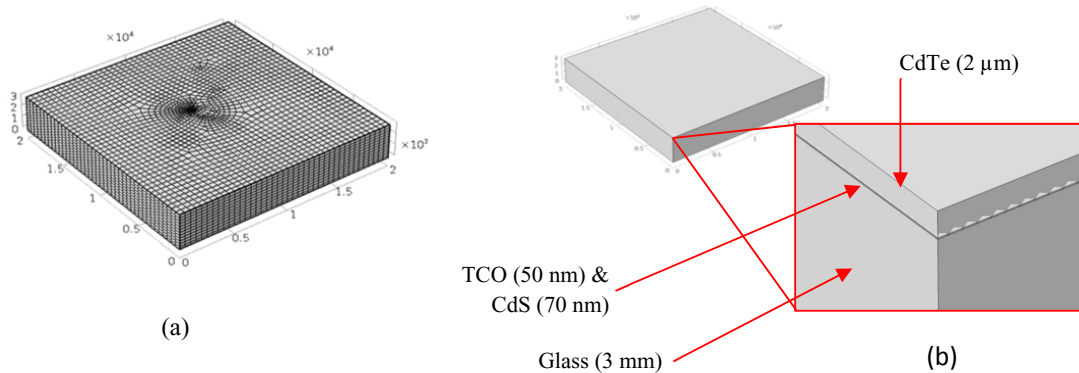


Figure 3: Images showing (a) solar panel mesh and (b) the panel geometry with the thicknesses of the various layers. Dimensions are given in  $\mu\text{m}$ .

A cubic swept mesh was used, with the element size set as a function of beam width, giving 14 elements across the beam width and approximately 134,000 elements in total. Laser beam widths were set at 5 mm with a 2 mm/s traverse rate. Correlation of CdTe  $n$  and  $k$  values with wavelength show very little change between wavelengths of 650 – 850 nm [16]. The mean values of  $n$  and  $k$  are 2.878 and 0.091 respectively. Using Fresnel relationships and assuming a  $0^\circ$  angle of incidence, CdTe absorptivity at 808 nm wavelength was calculated to be approximately 76%. This value was used in simulation.

### 3 Experimental setup

Laser experiments were conducted using an 808 nm diode laser, rated at a maximum output of 35 W, with a 1.5 mm long 100  $\mu\text{m}$  core fibre optic output. This was connected to a collimator which produced a near-perfect Gaussian beam output. Figure 4a shows the laser mounting and cooling system, and Figure 4b shows the optical setup. The collimator was set to give a  $1/e^2$  diameter of 5 mm, equal to the simulated Gaussian beam diameter. Process monitoring was achieved via use of a FLIR Thermovision A40 high-temperature thermal camera. The recorded temperature data was then analysed and process temperature profiles plotted.

Two sets of Gaussian experiments were completed, at power levels of 11 W and 5 W, with scanning velocities of 4 and 11 mm/s respectively:

- The 11 W, 4mm/s combination was required in order to maintain a sufficient surface temperature while avoiding the tendency for thermal stresses created by the Gaussian temperature gradient to shatter thin samples.
- The 5 W, 11 mm/s combination was used for simulation validations, in order to limit heating to the centre of the beam and increase the “contrast” between the centre and outer edges to get a clear reading of the temperature profile from the thermal camera. The simulation parameters were also modified accordingly.

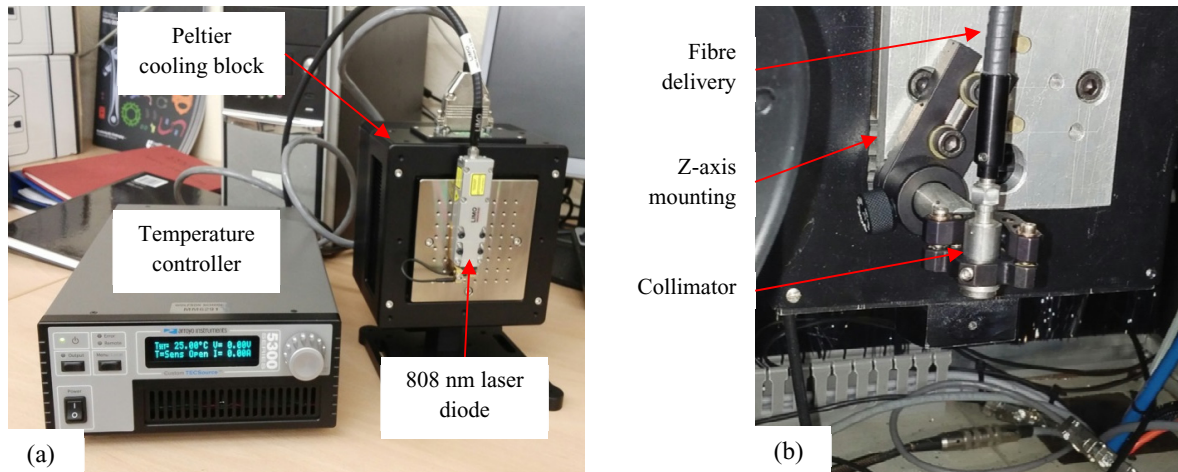


Figure 4: Images showing (a) laser diode setup and cooling system and (b) diode optical setup

The laser optics themselves were mounted on a manual Z-axis for beam focussing.  $MgCl_2$  treatment was carried out using an aqueous 1 M solution. The treatment was applied by dipping the samples in this solution before placing them in an insulated jig located on an x-y CNC stage for processing. The samples had a 2  $\mu m$  thick CdTe layer, as in the simulations.

#### 4 Simulation results

Beam shaping involved the alteration of a Gaussian beam profile into a pedestal beam and then into a rugby posts beam. Results were taken at the centre of the sample, in the middle of the process. 3D isothermal contours are shown in Figure 5. Simulations carried out here used a laser power of 10 W and a traverse speed of 2 mm/s.

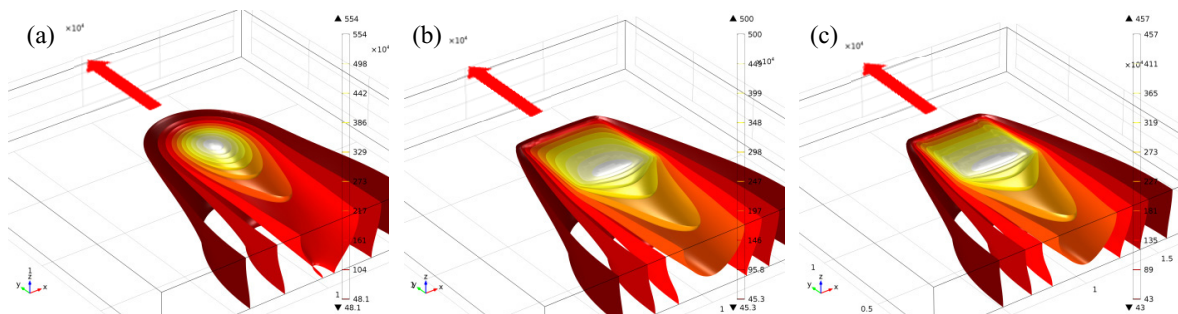


Figure 5: 3D temperature isothermal contours ( $^{\circ}C$ ) for (a) Gaussian beam (b) pedestal beam and (c) rugby posts beam. Red arrows indicate beam traverse direction. Dimensions are given in  $\mu m$  and temperatures in  $^{\circ}C$ .

These isotherms show that the primary improvement comes when a pedestal beam replaces the Gaussian beam. The beam footprint is now rectangular, which reduces the taper in the temperature profile after the beam has passed over. Although the maximum temperature is reduced from  $554^{\circ}C$  in the Gaussian to  $500^{\circ}C$  in the pedestal, this temperature is maintained over a much greater proportion of the width in the pedestal simulation, which leads to higher quality annealing. The rugby posts beam is an optimisation of the pedestal beam. Another slight reduction in maximum temperature is present, to  $457^{\circ}C$ , but this beam profiles reduces the majority of the remaining curvature

that was present in the pedestal beam and makes the thermal profile even more uniform.

Two-dimensional cross-sections were also created for the three beam profiles, in order to better present the relative uniformity of the different temperature profiles through the thickness of the panel. These are shown in Figure 6. They also show that to maintain the surface layer at the correct temperature, the power input is high enough to cause a level of temperature penetration into the substrate. The variations in surface temperatures between the different beam types suggest that this penetration is unavoidable, since reducing the energy density merely reduces the surface temperature; this cannot be allowed to occur if the annealing process is to be effective.

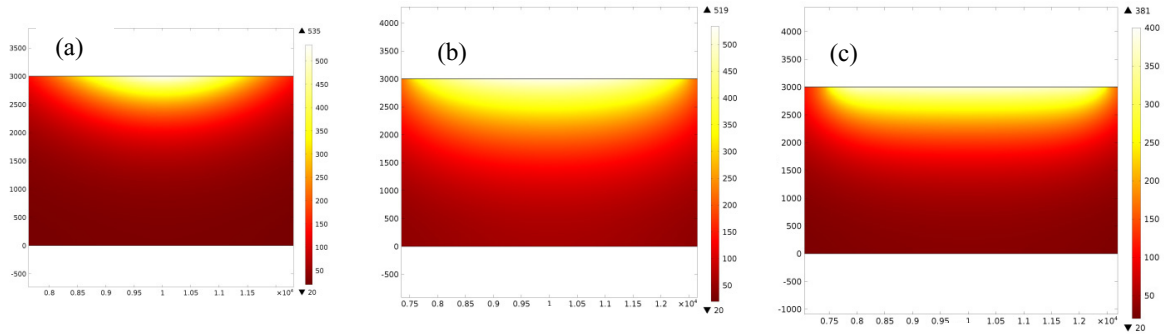


Figure 6: 2D temperature profiles (°C) for (a) Gaussian beam (b) pedestal beam and (c) rugby posts beam. Dimensions are given in  $\mu\text{m}$  and temperatures in  $^{\circ}\text{C}$ .

Results in Figure 6 show that when a pedestal beam is applied, the uniformity of the beam increases the effective width of the annealing zone, because greater levels of heat are applied to the edges. Whereas in the Gaussian beam the edges are heated by heat conduction from the centre, the pedestal beam applies this heat directly. The pedestal temperature profile is still curved and therefore non-uniform however. This is compensated for by the rugby posts beam, which more heat at the edges than the centre. This compensates for the greater levels of heat loss at the edges, as well as slightly increasing the width of the heat affected zone.

For each beam type, a single isothermal contour was plotted at  $200^{\circ}\text{C}$ . These were then combined on the same axis, as shown in Figure 7.

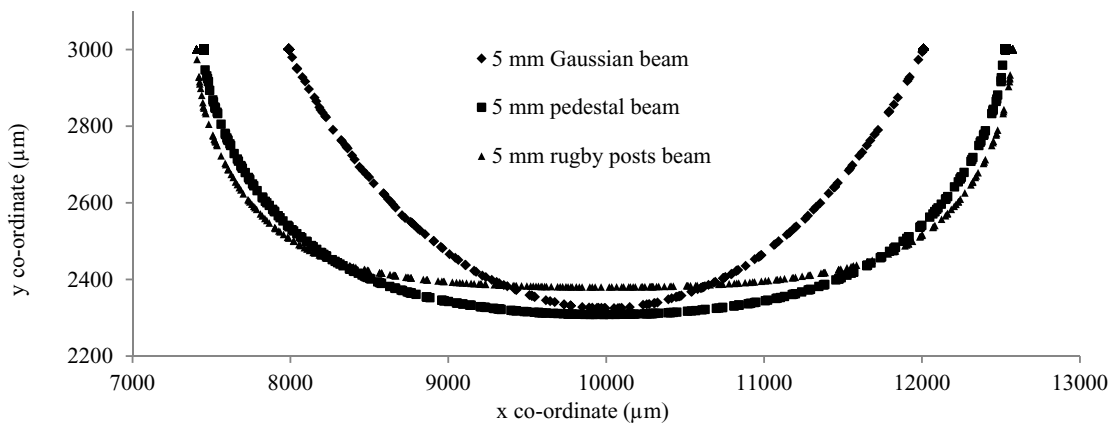


Figure 7: 2D isothermal plots for 5 mm Gaussian beam, pedestal beam and rugby posts beam

These plots show the relative curvature of the difference temperature profiles. It reveals the major improvements

that appear when a simple pedestal beam is used. The pedestal temperature profile is widened by approximately 500  $\mu\text{m}$  on either side. Although the pedestal temperature profile is still curved, the degree of curvature is greatly reduced and the temperature profile is much more uniform in depth. This tendency can be further optimised by the use of a rugby posts beam, where the width and profile at the edges are similar to the pedestal beam, but curvature at the centre is effectively eliminated.

## 5 Experimental results

Experimental results and synergy with simulations are presented here.

### 5.1 The effectiveness of the laser process

TEM analysis of pre-treatment samples confirmed high instances of stacking faults and other defects in the microstructure. These were present in all grains and are shown in Figure 8.

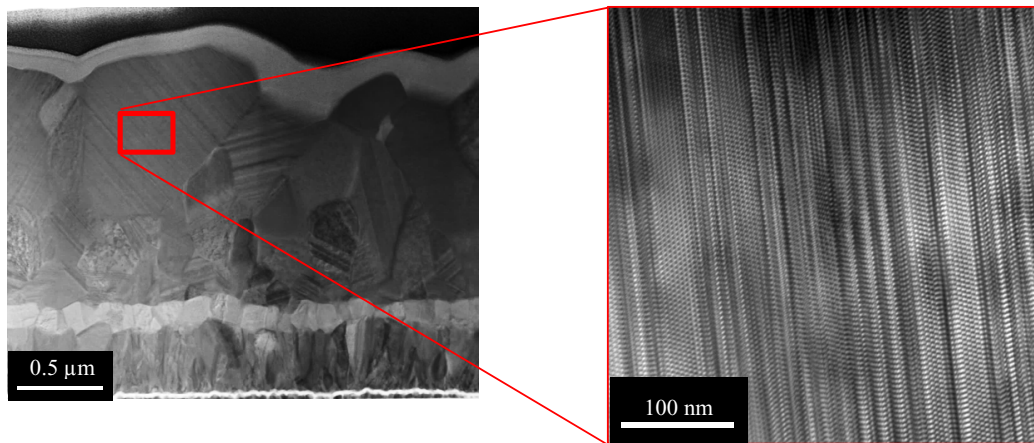


Figure 8: Pre-treatment CdTe sample showing high density of stacking faults

Annealing with a laser power of 11 W at a traverse rate of 4 mm/s showed that some defects were still present. Microstructural analysis of the post-treatment samples did reveal however, that there was evidence of the onset of recrystallisation of the CdTe layer near the top surface of the sample. There was also a visible reduction in the number of stacking faults; so the laser process was effective, albeit not totally, in the removal of these. This is shown in Figure 9.

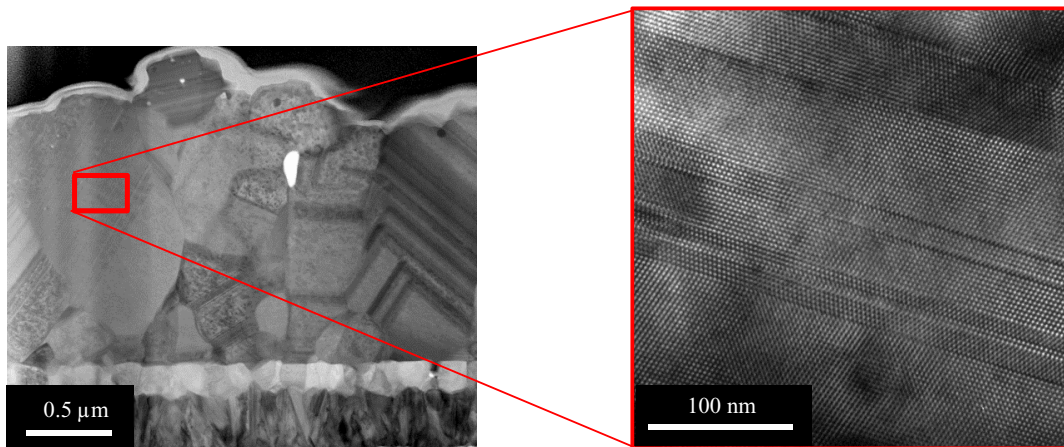


Figure 9: Post-treatment CdTe sample showing high density of stacking faults

A more detailed materials analysis of these results is presented by Lisco *et al.* [17].

### 5.2 Validation of simulations

Thermal camera results were used to compare the physical temperature profile. Physical experiments had shown that temperature build-up had a tendency to flatten the reading from the camera. Temperatures were plotted along lines located on the top surface of the sample traverse and longitudinally to the direction of beam traverse for both simulated and experimental results. The resulting plots are compared in Figure 10.

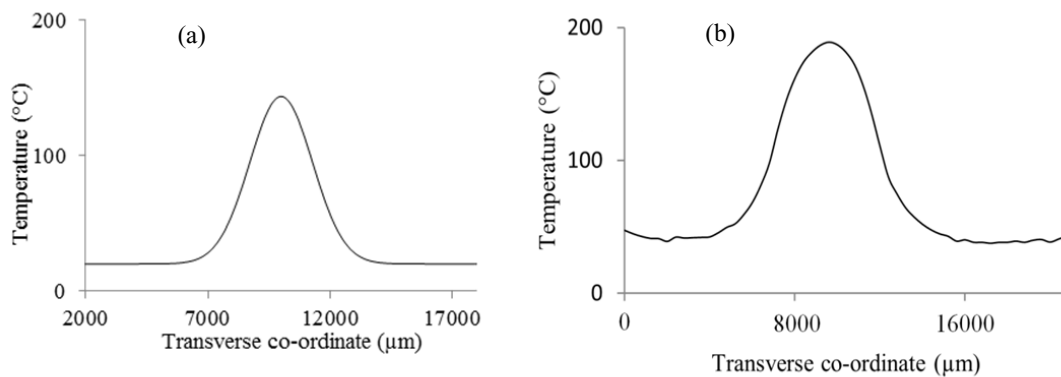


Figure 10: Graphs showing surface temperature profile of (a) simulated result and (b) experimental result

The experimental results are broadly similar in temperature profile to the simulated results. The shapes of the temperature profiles broadly follow the profiles of the laser beams. The difference between the two in this respect can be accounted to the fact that the laser beam is not a perfect Gaussian profile, so does not resemble the simulated beam exactly. Although the temperatures in the experimental results vs. the simulated results are different, they are in a very similar range to each other. This suggests that the differences lie in the details of the two processes experimental process; for example, minor variations in experimental sample size or inaccuracy in the simulated



material properties.

## 6 Concluding remarks

In this work investigations have been presented in the use of altered laser beam thermal profiles for annealing of CdTe.

Simulation results have shown that optimisation of laser beam profiles gives superior heating of the substrate. When a pedestal beam is used, it provides a considerable increase in the uniformity of the thermal profile. This gives several benefits. Firstly the thermal cycle undergone by the CdTe is much more consistent across the width of the laser track. This means that the post-annealing properties of the CdTe layer will be much more uniform with a pedestal beam than a Gaussian beam. Secondly, although the beam widths are equal, the *effective* width of the pedestal beam is considerably greater than the Gaussian beam. This is obvious in Figure 7, where the pedestal temperature profile is considerably wider than the Gaussian. In practice, this would allow faster processing with the pedestal beam since, with all other things being equal, it can anneal a greater area of panel at a time.

Further simulation development has shown that the CdTe temperature profile can be further optimised by use of a rugby posts beam profile. This places additional heat at the edges of the beam and counteracts the remaining curvature that is still present in the pedestal beam. This does not make the heat affected zone wider, but provides further improvements in temperature uniformity; showing its potential to optimise laser processing.

Laser annealing experiments were successful in annealing the CdTe layer. Analysis comparing pre-annealed CdTe vs. post-annealed CdTe showed that the laser process effectively removed stacking faults from the grains. Recrystallisation of the CdTe was also found in the region close to the top surface of the semiconductor layer. Although further development is necessary, results obtained so far show that laser annealing is a viable process.

Initial comparisons between simulated predictions and experimental results showed broad similarity between the two. The temperature distributions followed the same profile, which corresponded to the shape of the beam. In the case of the experimental plot, the beam is not perfectly Gaussian and this is reflected in the shape of the temperature plot. Temperatures were slightly higher in the experimental result, which suggests that the simulation is broadly accurate, with discrepancies due to minor inaccuracies such as differences in material reflectivity or sample size between the experimental and simulated tests. These results show that, while improvements are necessary, the simulation design is robust and reflective of the physical reality.

HOE development for 808 nm laser processing is currently underway and once complete these optics will be used to assess whether the predicted improvements in complex beam simulations can be replicated in experimental practice.

## References

- [1] Velumani TVS, Sakthivel SGK. Band structure and Optical properties CdTe and CdSn<sub>3</sub>Te<sub>4</sub> thin films 2008;273–7. doi:10.1063/1.2927567.
- [2] Ferekides C, Britt J. CdTe solar cells with efficiencies over 15%. Sol Energy Mater Sol Cells 1994;35:255–62. doi:10.1016/0927-0248(94)90148-1.
- [3] Yoo S-H, Butler KT, Soon A, Abbas A, Walls JM, Walsh A. Identification of critical stacking faults in thin-film CdTe solar cells. Appl Phys Lett 2014;105:062104. doi:10.1063/1.4892844.
- [4] Romeo A, Batzner DL, Zogg H, Tiwari AN. Recrystallization in CdTe / CdS 2000;362:420–5.
- [5] Romeo A, Ba DL, Zogg H, Vignali C, Tiwari AN. Influence of CdS growth process on structural and photovoltaic properties of CdTe / CdS solar cells 2001;67:311–21.

- [6] Major JD, Treharne RE, Phillips LJ, Durose K. A low-cost non-toxic post-growth activation step for CdTe solar cells. *Nature* 2014;511:334–7. doi:10.1038/nature13435.
- [7] Spalatu N, Hiie J, Valdna V, Caraman M, Maticiuc N, Mikli V, et al. Properties of the CdCl<sub>2</sub> Air-annealed CSS CdTe Thin Films. *Energy Procedia* 2014;44:85–95. doi:10.1016/j.egypro.2013.12.013.
- [8] Johnson DR. Microstructure of electrodeposited CdS/CdTe cells. *Thin Solid Films* 2000;361-362:321–6. doi:10.1016/S0040-6090(99)00779-8.
- [9] Potter MDG, Halliday DP, Cousins MA. Analysis of CdCl<sub>2</sub> annealing process in CdTe/CdS solar cells. 16th Eur. Photovolt. Sol. Energy Conf., 2000, p. 847–50.
- [10] Abbas A, West GD, Bowers JW, Isherwood P, Kaminski PM, Maniscalco B, et al. The Effect of Cadmium Chloride Treatment on Close-Spaced Sublimated Cadmium Telluride Thin-Film Solar Cells. *IEEE J Photovoltaics* 2013;3:1361–6. doi:10.1109/JPHOTOV.2013.2264995.
- [11] Kim N-H, Park C Il, Lee H-Y. Microstructure, stress and optical properties of CdTe thin films laser-annealed by using an 808-nm diode laser: Effect of the laser scanning velocity. *J Korean Phys Soc* 2013;63:229–35. doi:10.3938/jkps.63.229.
- [12] Kim N-H, Park C Il, Park J. A pilot investigation on laser annealing for thin-film solar cells: Crystallinity and optical properties of laser-annealed CdTe thin films by using an 808-nm diode laser. *J Korean Phys Soc* 2013;62:502–7. doi:10.3938/jkps.62.502.
- [13] Duley WW. *Laser Welding*. John Wiley & Sons Ltd.; 1999.
- [14] Kell J, Tyrer J, Higginson R, Jones J, Noden S. Laser weld pool management through diffractive holographic optics. *Mater Sci Technol* 2011;28. doi:10.1179/1743284711Y.0000000050.
- [15] Goffin N, Higginson R, Tyrer J. The use of Holographic Optical Elements (HOE's) to investigate the use of a flat irradiance profile in the control of heat absorption in wire-fed laser cladding. *J Mater Process Technol* 2015. doi:10.1016/j.jmatprotec.2015.01.023.
- [16] Palik E. *Handbook of Optical Constants of Solids*. Harcourt Brace Jovanovich; 1985.
- [17] Lisco F, Goffin N, Abbas A, Claudio G, Woolley E, Tyrer J, et al. Laser Annealing of thin film CdTe solar cells using a 808 nm diode laser. *Photovolt. Spec. Conf., Portland: 2016 IEEE 43rd; 2016, p. In press.*